25th ABCM International Congress of Mechanical Engineering
October 20-25, 2019, Uberlândia, MG, Brazil

# COB-2019-2088
# DEVELOPMENT OF A THERMAL SPRAY SYSTEM USING A LONG ARC PLASMA TORCH

**Roberson José da Silva**
**Felipe de Souza Miranda**
**Homero Santiago Maciel**
**Gilberto Petraconi Filho**
Instituto Tecnológico de Aeronáutica, São José dos Campos, SP, Brasil
roberson123@gmail.com, mirannda.fs@gmail.com, odairtur@gmail.com, petrafilho@gmail.com

***Abstract.*** *Thermal plasma spray is a technique for coating thick films by scattering of molten particles (metallic or ceramic powders) in high temperatures and velocities. That is, molted particles are accelerated towards the surface of the sample, where they are solidified to form a thick protecting layer. This process is used to obtain layers of high thermal and mechanical resistance, which confers high protection in aggressive ambient, which are found, for example, in the reentry atmosphere or in turbine blades. Conventional systems use a plasma torch that operates with short arcs, currents in the order of hundreds of amperes and tens of volts. This work shows the development of a thermal plasma spraying system using a reverse vortex plasma torch, which works with long arc, currents of the order of a hundred amperes, and some hundreds of volts. The system characteristics and control parameters to obtain the necessary heat to melting the alumina powder, in order to obtain the ceramic coating are presented.*

***Keywords:*** *ceramic coating, plasma torch, powder spray, thermal shield, thermal spray*

## 1. INTRODUCTION

Plasma spray is commonly used in many industrial sectors, including aeronautics, energy, automotive, mining, biomedical and electronics (Tucker Jr., 2013). Plasma spray deposition technique is a well-established technology for surface treatment and modification in coating synthesis by stacking lamellae resulting from impact, flattening and solidification by the collision of molten particles (Miranda et al., 2018). Plasma spray is probably the most versatile of all thermal spraying processes, because there are few limitations of materials that can be sprayed, and few limitations on the material, size and shape of the substrate (Fauchais, 2004). The coatings are characterized by a highly anisotropic lamellar structure. Further, stacking of the particles generates specific interlamellar characteristics within the structure, especially voids, which may or not connect through the particles encountering the coating thereafter. In this context, taking into account the versatility of plasma spray processes, the purpose of thermal spray coating is to obtain layers of high thermal and mechanical resistance (characteristic of materials with high melting point) with the lowest possible compromise of the substrate (Solonenko, 2003; Pawlowski, 2008; Fauchais et al., 2014). Figure 1 shows a typical system of thermal plasma spray (Xie et al., 2004). As can be seen, a thermal plasma spray system has three functional parts: the plasma torch, the powder feeder and a spraying positioning system.

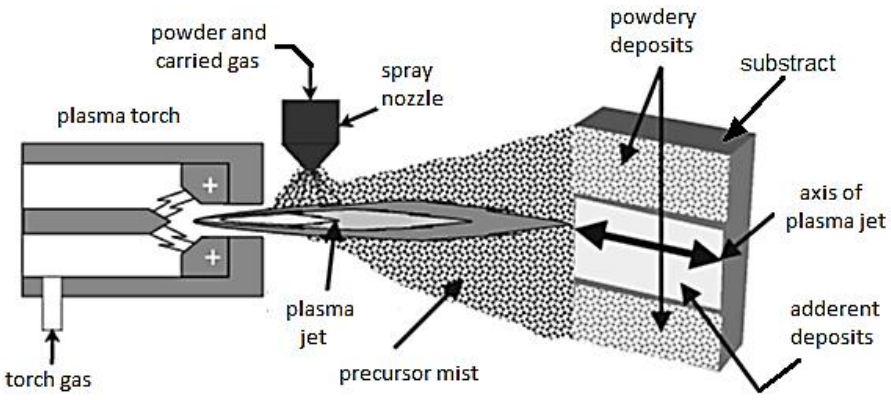


Figure 1. Basic scheme of thermal plasma spray to powders

### 1.1 Tornado Plasma Torch

Plasma torches are devices used to stabilize an electric discharge with gas flow, aiming at the conversion of electric energy into thermal energy. In a thermal plasma torch, operating from electric discharge, high enthalpy plasma results from the interaction of the gas with the electric arc. The study of electric discharges in gases and formation of the plasma jet involves phenomena of gas dynamics, mass and heat transfer, electro- physical and aero-thermodynamic processes (Solonenko, 2003).

Conventional plasma torches used in thermal spray systems operate with short arcs as shown in figure 2a, 20–100 V and 300–1000 A. These currents require the use of robust cathodes, usually of rubidium or tungsten, materials that can only work in non-oxidizing environments and thus these torches are restricted to working with inert gases like argon (Fauchais et al., 2014). Another possibility presented in this work is the use of a plasma torch that operates with a long arc as shown in figure 2b and therefore works with a higher voltage in the range of 100–400 V and lower currents at about 150 A (Silva, 2011). Working with smaller currents, this torch can also use smaller cathodes, which operate with a concentrated arc, called a hot cathode. These cathodes are made of copper with hafnium insert, which can operate in an oxidizing environment using air as working gas. The elongation of the arc occurs due to the vortex flow to which the working gas is subjected when entering the torch.

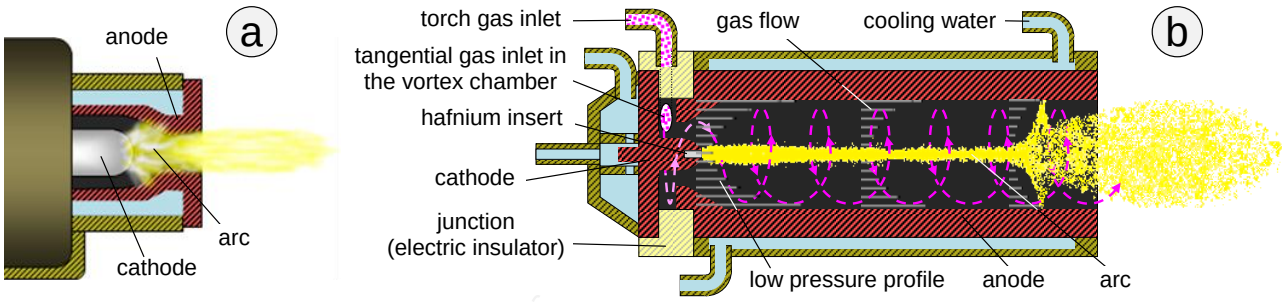


Figure 2. Schematic: conventional short arc torch (a) and long arc torch stabilized by vortex (b)

The Tornado torch presents a more elaborate concept to long-arc torch as shown in figure 3. It has an elongated cathode that is traversed by two coaxial gas layers that move in helical flow with the same direction of rotation but at opposite axial directions. The anode (14) has an inner diameter smaller than that of the cathode (4). This forces the gas leaving the vortex chamber (13) with centrifugal acceleration to be directed in helical flow, close to the electrode wall to the bottom of the cathode. When the gas reaches the cathode bottom wall the helical flow maintains the direction of rotation but reverses the direction of axial propagation. At lower angular velocity, the helical flow radius is reduced and passes through the anode channel towards the torch gas outlet. Like the example in figure 2b, the helical flow creates the low pressure channel that stabilizes the arc in the torch axial axis. Then the arc is elongated from the hot cathode (3) to the middle of anode channel, closing the electric circuit. After this point the heated and still ionized gas expands into the outlet of the torch forming a plasma plume (18). The advantage of this concept approach is that the double layer of gas provides a greater thermal insulation between the arc and the electrode, increasing the thermal efficiency of the torch (Silva, 2011).

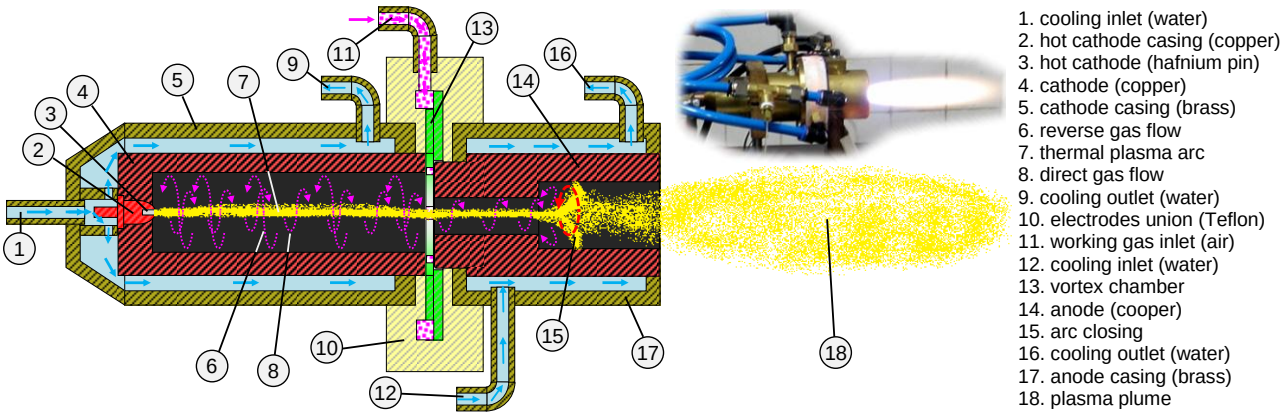


Figure 3. Schematic of Tornado plasma torch

Each temperature corresponds to a specific enthalpy in the gas as showed in figure 4 (P. Fauchais; M. I. Boulos and E. Pfender, 1994). The specific enthalpy of 6.6 MJ/kg in air, e.g., corresponds to the temperature of 3,800 K (~ 3,500 °C). Thus, it is possible to adjust gas temperature at the torch nozzle by changing its operating point to a corresponding specific enthalpy for the working gas.

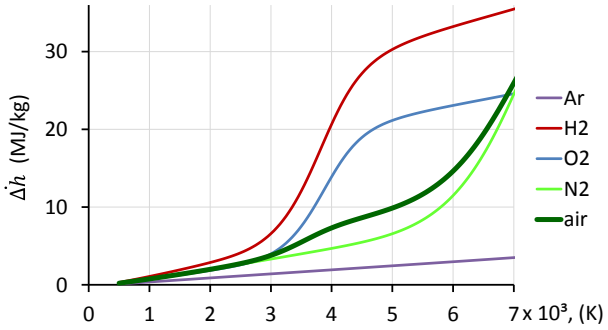


Figure 4. Specific enthalpy of gases as function of plasma temperature

### 1.2 The powder sprayer

The carrying of the powder to the plasma torch nozzle was performed by a powder feeder PFV-101 of the Tekna (Québec, CAN) which uses the vibration principle to control feed of the powder (figure 5). It consists of a vibrating feeding module (a) and a control box (b). The equipment works with internal pressure of up to 1 bar and is used for fine powders, 0.5–500 μm, and powder spray rates of 0.1–5 kg / h. In this equipment, a bowl containing a helical path through which a powder fillet runs and rises until it falling in a hole in the top of the bowl where powder is taken to outlet of vibration feeder by the carrier gas (air). Spray control is performed by adjusting of the gas flow rate, frequency and intensity vibration of a bowl within the vibrating feeder. The powder flow rate is defined by setting of frequency and intensity of vibration.

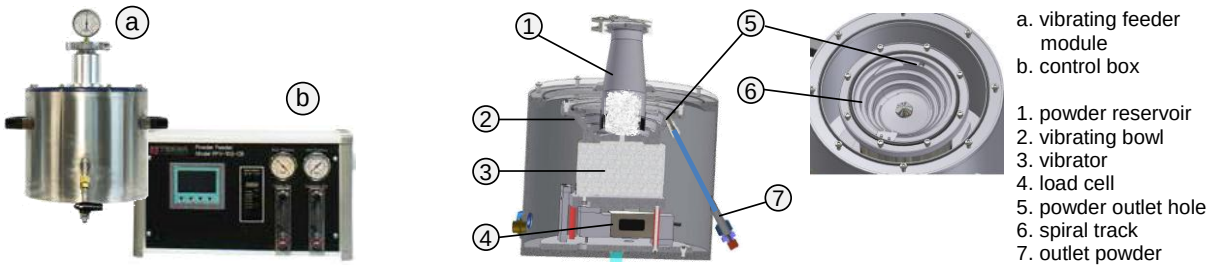


Figure 5. PFV-101 model vibrating powder feeder from Tekna

## 2. MATERIALS AND METHODS

### 2.1 Materials

The objective of this work is the development of the plasma thermal spray system for ceramic powders, then basic materials were chosen to perform the tests. The ceramic powder used in the tests was alumina with particle size of 70 to 210 μm. The alumina has a melting point of 2,072 °C (Patnaik, 2003). This alumina was previously heated in an oven at 60 °C for 4 hours and then sieved to define this range of granulometry. The substrates used in the thermal spray tests were ANSI 304 stainless steel, disk-shaped of 45 × 4 mm.

### 2.2 Plasma jet temperature

In the initial configuration the gas temperature at outlet nozzle of the torch was 3,500 ° C, already above the melting point of the alumina (2,072 ° C). Thus, initial attempts of coating in this configuration were performed, but without success. An issue to be considered is that the alumina melting will only occur if the powder particle remains resident in the heated gas until it has sufficient energy for the melting. The time required will depend on how much above the melting point is the gas temperature, the thermal gas interaction and the particle size. The plasma jet temperature of 3,500 °C consists of an estimate of the mean value of the gas temperature in the torch nozzle. This

temperature decreases as a function of the radial distance of the shaft and also as a function of the axial distance of the torch nozzle. It is necessary to optimize the plasma jet energy concentration and the residence time of the powder particle in the hottest region of the jet for the melting occur. The molten powder grains also need to be fast enough that, upon sticking to the substrate, an adhered splat is formed. These splats are accumulating, solidifying and forming overlapping layers up to the thickness desired for the coating. The dispersion of the powder in the plasma jet will be reflected in the temperature and grain velocity variations and, consequently, in the uniformity of the microstructure of the coating obtained (Xie et al., 2004). To address these issues, the torch anode has been changed to radially concentrate the heat from the plasma jet. A copper insert was inserted by reducing the internal diameter to 6 mm, as shown in figure 6.

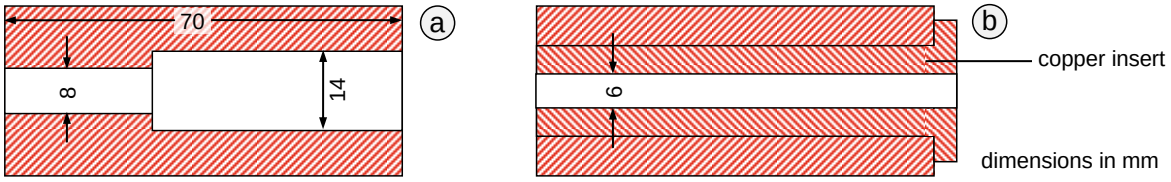


Figure 6. Anodo original (a) and anodo modificado (b)

With the modified anode, a specific enthalpy mapping was performed by varying the arc electric current and the working gas (air) flow rate whiting operating limits of plasma torch (Silva, 2011). The specific enthalpy for each operating point was obtained with equation

$$\Delta\dot{h} = \frac{P_{\text{ef}}}{G_g} \tag{1}$$

where $G_g$ is the working gas flow rate in kg/s and $P_{\text{ef}}$ is the thermal power effectively delivered to the plasma jet in W. The effective power was obtained with equation

$$\mathrm{P_{ef}} = \mathrm{P_{arc}} - \mathrm{P_{cooling}} \tag{2}$$

where $P_{arc}$ is the electrical power in W, which is converted to heat by arc and $P_{cooling}$ is the lost power to electrodes wall of torch W and which it is transferred to cooling water. The electric power of arc was obtained with equation:

$$\mathrm{P_{arc}} = \mathrm{V} \cdot \mathrm{I} \tag{3}$$

where V is the voltage in V and I is the electrical current in A provided by the power source to arc in the plasma torch. The lost power heats the cooling water and thus can be obtained by equation

$$\mathrm{P_{cooling}} = G_w \cdot C_{p\,w} \cdot (T_{in} - T_{out}) \tag{4}$$

where $G_w$ is the flow rate of cooling water in kg/s, $C_{p\,w}$ is the water specific hot in cal·kg$^{-1}$·°C$^{-1}$, $T_{in}$ is the water temperature when entering the torch in °C and $T_{out}$ is the water temperature coming out of the torch.

The outlet of the cooling water in the cathode is connected to the cooling inlet of the anode so that all the lost energy to torch cooling is considered by the measurement of $T_{in}$ and $T_{out}$ temperatures. These temperatures were measured with thermocouples that were adapted in the water inlet of cathode and in the water outlet of the anode. The water flow rate was measured with rotameter and was adjusted to values that would promote water heating between 5–15 °C. The arc electric current was converted into a voltage signal by a current shunt of 0.6 mV/A. The arc voltage was converted to current proportional to 0-1 mA by a resistor of 800 kΩ. This signals was processed by a protection circuit and they was converted to 0–1.5 V proportional to current 0-150 A and 0–2 V proportional to voltage 0–800 V, respectively. Voltage, current, and temperature signals were measured by the National Instruments acquisition modules controlled with LabView language programing. For voltage and current signals was used a NI USB-6009 acquisition module. For temperature signals was used a NI cRIO-9211 + NI USB 9162 set that is specific for acquisition of thermocouple signals.

### 2.3 Powder flow rate control

A study was performed with the powder feeder to map the variation of the powder rate as a function of the frequency and intensity of the vibration. The test setup that was performed is shown in figure 7. In this setup the outlet

hose of the carrying gas and powder (10) is directed to a closed Becker (12). The closing is performed with a porous fabric (11) which retains the powder but allows exhausting gas (air). This is necessary for the reuse of the powder in the several cycles witch was performed to the mapping. The vibration feed module (9) has a load cell which constantly measures the weight of the vibratory set (vibrator, bowl with spiral track and powder reservoir) and it sends to CLP (programmable logic controller) inside control box (5). When vibrating the bowl, a row of powder rise up the spiral track and falls in the outlet hole at track end. The powder row that going carrying out decreases the weight of the set measured by the load cell. PLC calculates the mass variation as a function of time and reports the powder flow rate in the display of control module (5).The control module also provides the weight and powder flow rate values in the form of 4-20 mA analog signals on a rear connector. These signals were acquired by a National Instruments NI-6009 module (3) controlled with LabView language programing on a computer (1).

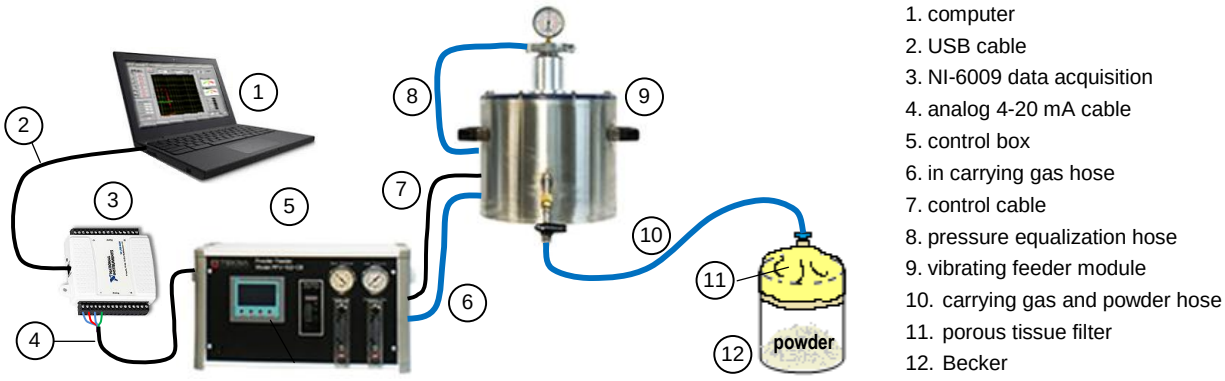


Figure 7. Setup for powder flow rate control mapping of the vibrating feeder

As the weighing occurs over the entire vibrating set it is subject to vibration disturbance which is propagated for the measurement of the powder load weight. Although the PLC program in the control module already contains a filtering routine, the flow rate indicated by the powder feeder is still very unstable. Thus, it was necessary adding more filtering steps to obtain a flow rate value that was applicable. It was added an analog LPF (low pass filter) at signal input of data acquisition module and a digital filter in the Labview program. The analog filter was obtained by adding a 3,300 µF capacitor to the input of the data acquisition module that has an input impedance of 220 Ω performing a 0.22 Hz LPF filter. The digital treatment was carried out in two stages: the first with the addition of a digital LPF of 0.1 Hz and the second a scan filter with polynomial adjustment of 2nd order of 40 values. As the powder flow rate is given by $d_w/d_t$, this value is obtained by computing the derivative ($W' = a_1 + a_2 t$) of the 2nd stage polynomial ($W_{LPF} = a_0 + a_1 t + a_2 t^2$), using its coefficients which are fitted point to point during the sweep. Figure 8 shows the values obtained with the filtering processes, where m is the mass provided by powder feeder analog signal and filtered by the analog LPF, m* is the mass value processed by the digital filter, G is the powder flow rate calculated and provided by feeder analog signal and G* is the powder flow rate processed by the digital filter. It is possible to verify 3 distinct regions in the evolution of the powder flow rate: initial rise (A), plateau (B) and final peak and fall (C). The regions boundaries A-B and B-C were defined at time when 20 and 70% of powder reservoir consumption, respectively occur. In the plateau region was performed a linear adjustment with G* values obtaining a mean line. The points $G_{min}$ (minimum flow rate) and $G_{max}$ (maximum flow rate) are defined by crossing this mean line with the boundaries of the regions. Region B was defined as the region useful to working with this powder feeder.

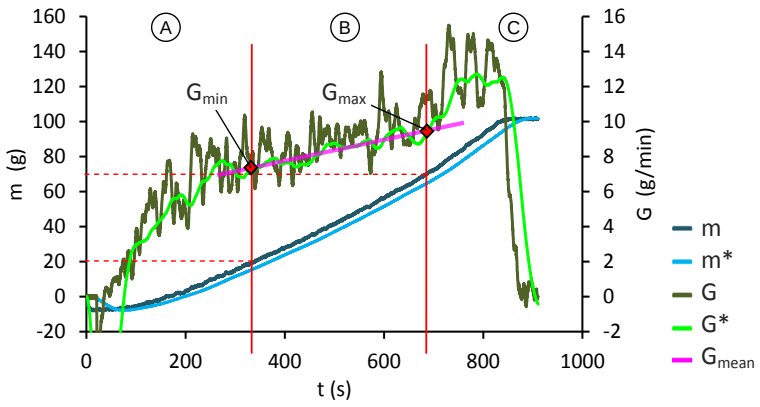


Figure 8. Flow rate and powder mass after filters and definition of the useful region (B) to working

O procedure shown in Figure 8 was repeated for the mapping of the powder flow rate as a function of frequency and intensity of vibration. All the tests were performed with 100 g of alumina powder in the reservoir. The carrying gas flow rate was adjusted at 6 L/min. The mapping of the flow rate as function of intensity of the vibration was performed at frequency in 114.8 Hz. This is frequency value which adjusted to initiate powder movement with the lowest vibration intensity possible (as defined in the PFV 101 manual).

### 2.4 Powder injection nozzle

The injection of powder into the plasma jet was performed by a nozzle with a hole of 2 mm diameter. A device with a joint attached to the torch front allowed the positioning of the powder flow directed at the outlet of plasma jet at about 45°, as shown in figure 9. The purpose of this incident angle was to provide a velocity component contrary to the flow of the plasma jet. In this way, the powder particle first approaches the point of greatest gas enthalpy at the plasma jet outlet and only then reverses the trajectory towards the substrate direction, thereby increasing its residence time in the plasma jet.

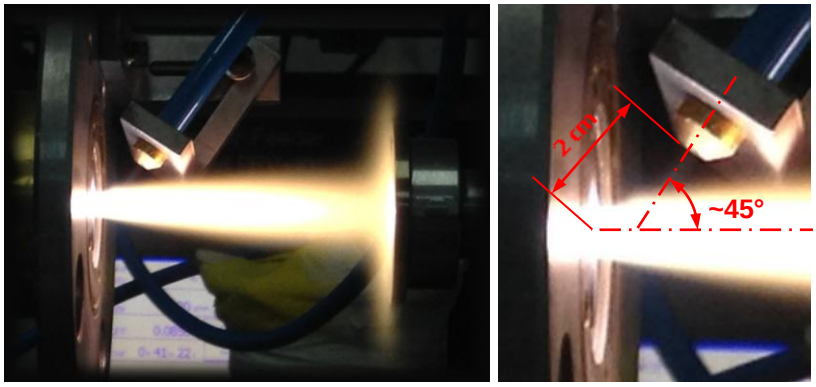


Figure 9. Powder injection nozzle and plasma jet

### 2.5 Powder thermal spray setup

Figure 9 shows the powder thermal spray test running a deposition. The substrate sample is fixed on an aluminum sample holder that is attached on end of a cooled lever arm. This set is attached on an X-Y axis automatic system that positions the sample at a determined distance from the plasma torch nozzle (figure 13).

### 2.6 Velocity and temperature of the powder particles

The velocity and temperature of the powder particles ejected during the thermal spraying process were measured by an optical analyzer model DPV 2000 manufactured by Tecnar as setup shown in figure 10. This equipment consists of an X-Y scanning system (1) and an optical and computational processing system (2). The X-Y scanning system positions an optical sensor to better capture the flow of heated particles in sprinkling. The processing system has an optical particle detection system and a CPU with a dedicated program that performs statistical calculations to obtain temperature, velocity, particle size and other thermal spraying parameters (Mauer et al., 2013).

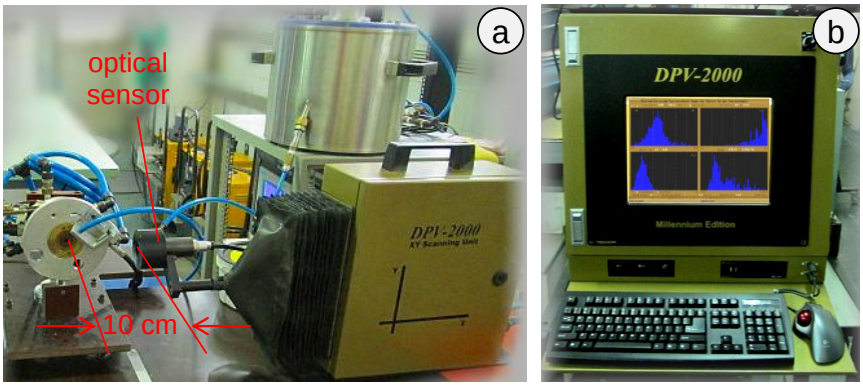


Figure 10. Setup to measuring thermal spray parameters

## 3. RESULTS

### 3.1 Mapping of the plasma torch temperature

The plasma torch was operated with an electric current of 76–110 A, gas flow of 80-200 L/min and the specific enthalpy obtained was 6.1–11.9 MJ/kg, corresponding to temperatures of 3.6–5.5 × $10^3$ K. Figure 11 shows the mapping of gas temperatures as a function of electric current (I) and gas flow rate ($G_{air}$).

| $G_{air}$ (L/min) | I (A) | $\Delta\dot{h}$ (MJ/kg) | T (K) |
|---|---|---|---|
| 80 | 99 | 11.6 | 5,481 |
| 90 | 108 | 11.9 | 5,549 |
| 100 | 98 | 10.4 | 5,173 |
| 100 | 100 | 10.8 | 5,298 |
| 100 | 109 | 11.3 | 5,408 |
| 100 | 109 | 11.4 | 5,430 |
| 100 | 110 | 11.6 | 5,483 |
| 109.5 | 109 | 11.3 | 5,414 |
| 110 | 107 | 11.0 | 5,329 |
| 110 | 110 | 11.4 | 5,435 |
| 120 | 99 | 9.5 | 4,855 |
| 120 | 107 | 10.4 | 5,171 |
| 120 | 111 | 11.0 | 5,335 |
| 130 | 96 | 9.1 | 4,709 |
| 130 | 107 | 9.9 | 5,015 |

| $G_{air}$ (L/min) | I (A) | $\Delta\dot{h}$ (MJ/kg) | T (K) |
|---|---|---|---|
| 130 | 110 | 10.5 | 5,201 |
| 140 | 95 | 8.4 | 4,397 |
| 140 | 110 | 10.1 | 5,071 |
| 150 | 110 | 9.4 | 4,814 |
| 165 | 88 | 7.6 | 4,099 |
| 165 | 105 | 8.6 | 4,484 |
| 200 | 76 | 6.1 | 3,665 |
| 200 | 94 | 7.3 | 3,983 |

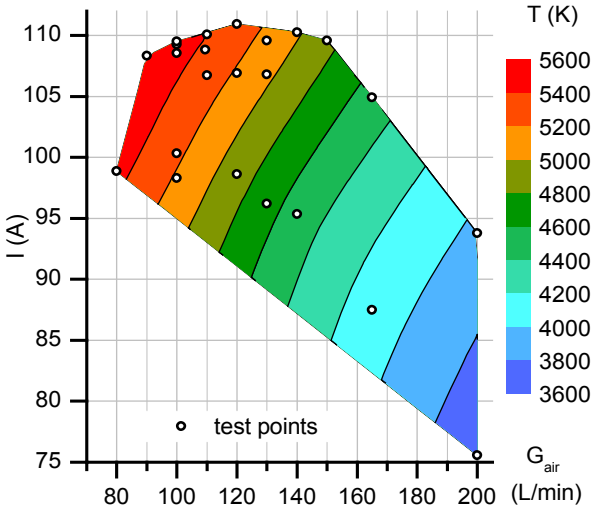


Figure 11. Mapping of gas temperature as a function of $G_{air}$ and I at plasma jet output

### 3.2 Mapping of the powder flow rate control

Figure 12 shows the powder flow rate results as a function of vibration intensity at 114.8 Hz (a) and as a function of frequency at 18% intensity (b). Based on results, the setting parameters to control powder flow rate were those which meet in the more linear regions of mapping profiles: vibration intensities below 18% and frequencies above 114.5 Hz.

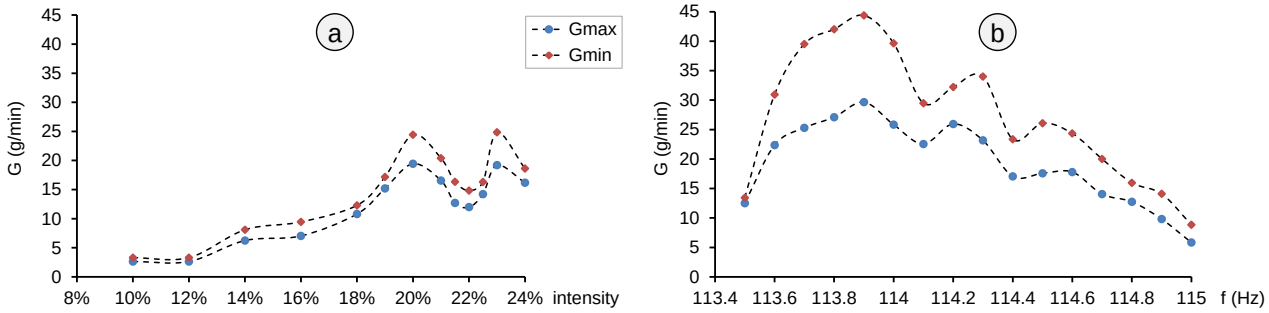


Figure 12. Powder flow rate as a function of vibration intensity (a) and frequency (b)

### 3.3 Optimization of deposition parameters

Deposition experiments were performed on the substrates changing the parameters of the thermal spraying. Table 1 shows the parameters used in each test where I is the electric current of the arc, G is the plasma gas flow rate, T is the plasma jet temperature at the torch nozzle, d is the distance from the substrate to the torch nozzle, t is deposition time, $i_{vib}$ is the vibration intensity of the powder feeder, f is the vibration frequency, $G_{powder}$ is the powder flow rate and $G_{carrier}$ is the flow rate of the powder carrying gas. Figure 13 shows the first test in progress. The orange coloration of the plasma occur due to interation of the alumina powder with plasma. The luminescent traces advancing in front of the jet plasma plume refer to the alumina powder particles (a). In ‘b’, it is shown the thermal spraying in progress with the deposition of the alumina on substrate.

Table 1. Experimental parameters of plasma thermal spray to optimization of the coating

| Test | Sample | I (A) | $G_{plasma}$ (L/min) | $T_{plasma}$ (K) | d (cm) | $t_d$ (s) | f (Hz) | $i_{vib}$ (%) | $G_{powder}$ (g/min) | $G_{carrier}$ (L/min) |
|---|---|---|---|---|---|---|---|---|---|---|
| #1 | A01 | 95 | 140 | 4,400 | 12 | 100 | 114.6 | 16.2 | 10–12 | 6 |
| #2 | A02 | 100 | 102.5 | 5,340 | 10 | 45 | 114.8 | 11.0 | 2–5 | 4 |
| #3 | A03 | 105 | 90 | 5,420 | 8 | 45 | 114.8 | 11.0 | 2-5 | 6 |
| #4 | A04 | 105 | 90 | 5,420 | 8 | 45 | 114.8 | 11.0 | 2-5 | 4 |
| #5 | A05 | 105 | 90 | 5,420 | 8 | 45 | 114.8 | 11.0 | 2-5 | 8 |
| #6 | A06 | 105 | 90 | 5,420 | 6 | 45 | 114.8 | 11.0 | 2-5 | 5 |
| #7 | A08 | 105 | 90 | 5,420 | 7 | 90 | 114.8 | 11.0 | 2-5 | 5 |

Note: The gray font refers to values that remained the same as in the previous test.

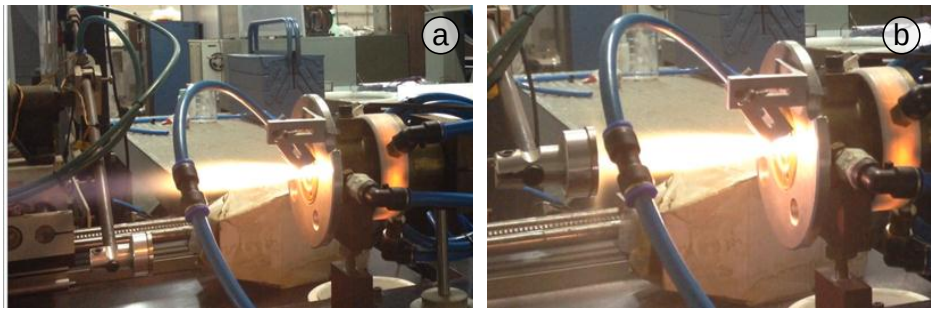


Figure 13. First coating by sprinkling of plasma running

Figure 14 shows the result of the coatings obtained in each condition of table 1. The magnifications of coatings were obtained using a ZEISS Axio Scope-A1 optical microscope. In Test #1 it is possible to verify that the coating obtained was irregular presenting peak regions with alumina accumulation and valley regions with some spots uncovered on the substrate. In valley regions is possible to identify a melting start of the alumina by the glassed aspect. In Test #2, the plasma temperature was increased, the substrate was approximated, and spray time and carrying gas flow rate were reduced. In this condition, it is possible to verify an intensification of the glassification aspect in the valley regions, as well as less pronounced peaks indicating an increasing of the melting powder process. In Test #3, the plasma temperature was increased, the substrate was approximated and the flow rate of the powder carrying gas was increased. In this condition was verified an increase of the glassification regions with fewer peaks of non-melted powder accumulation. In Test #4, only the carrying gas flow rate was decreased. Drastic reduction of the non-melted particles was verified, with predominance of glassified and translucent region, but thin and with spots uncovered. In Test #5, only the gas flow rate was increased. The coating stayed visibly thinner and with less peaks of alumina non-melted than previous coating. In Test #6 the substrate was neared torch and the flow rate of the carrying gas was reduced to a condition intermediate between #3 and #4 tests. In this condition, the thicker coating was obtained. However, during the cooling of the sample, there was delamination due to superheating of the substrate by the approximation of the plasma jet and also due difference of the thermal expansion coefficient between the metallic substrate and the alumina. In test # 7, the substrate was positioned 7 cm from the torch nozzle, the deposition time was doubled, and the cooling water flow was cut to the sample holder arm for slow cooling after deposition. During the deposition process occurred an overheating of the substrate leaving it incandescent (a). A thicker coating was obtained (b); however, about 1 min later a delamination occurred as in Test #6 (c).

In Test #6 and #7, it was verified that the delamination was accentuated by the substrate heating and cooling. In order to determine the threshold of this failure, multilayer coating tests were performed (Li et al., 2011), waiting 3 min to the cooling between depositions and limiting the exposure time of the substrate to the plasma jet heat flow to each coating layer. The parameters of the plasma torch and the powder feeder were maintained as in Test #7. Figure 15 shows the results of the coatings obtained with the setup and number of layers to each performed test. In Test #8 the deposition occurred in thin layers and followed until the $6^{th}$ layer when a delamination was observed. The Test #9 was a repetition of the previous test, but the delamination was observed soon after the $2^{nd}$ layer. This occurred until the $6^{th}$ layer. In Test #10, the deposition time per layer was reduced to 10 s to minimize the effect of heating on the substrate. Eight layers were deposited without delamination. Only a slight elevation was evident in the center of the deposition indicating the imminence of cracking. In Test #11, the substrate distance was reduced to 6.5 cm. The depositions occurred normally without apparent cracks, until the $6^{th}$ layer, when a small crack appeared. After the $7^{th}$ deposition a crack became evident. In Test #12, the deposition time was reduced to 9 s. After the $5^{th}$ layer, a slight crack appeared which became evident after $7^{th}$ layer. In Test #13, the deposition time was reduced to 8 s. After the $4^{th}$ layer, a slight elevation appeared and that was accentuated in the following layers. In Test #14 the deposition time was reduced to 4 s and 8 layers were deposited. The obtained coating was less thick than the previous test due to the reduction of

deposition time, however, no failure was observed between the layers depositions or after the process end. This was the deposition condition that obtained the best coating. For the following three tests, only the deposition time was changed to 5, 6 and 7 s, respectively, maintaining the other conditions. In Test #15, no crack was observed, only a slight elevation in the center of the deposition. In Test #16, it was verified a slight elevation after the 5th layer, which was accentuating until the 8th layer deposition, but no evident crack. In test #17, it was observed a slight elevation after 5th layer which was accentuating until the 7th deposition, when in the 8th deposition, the crack was evidenced.

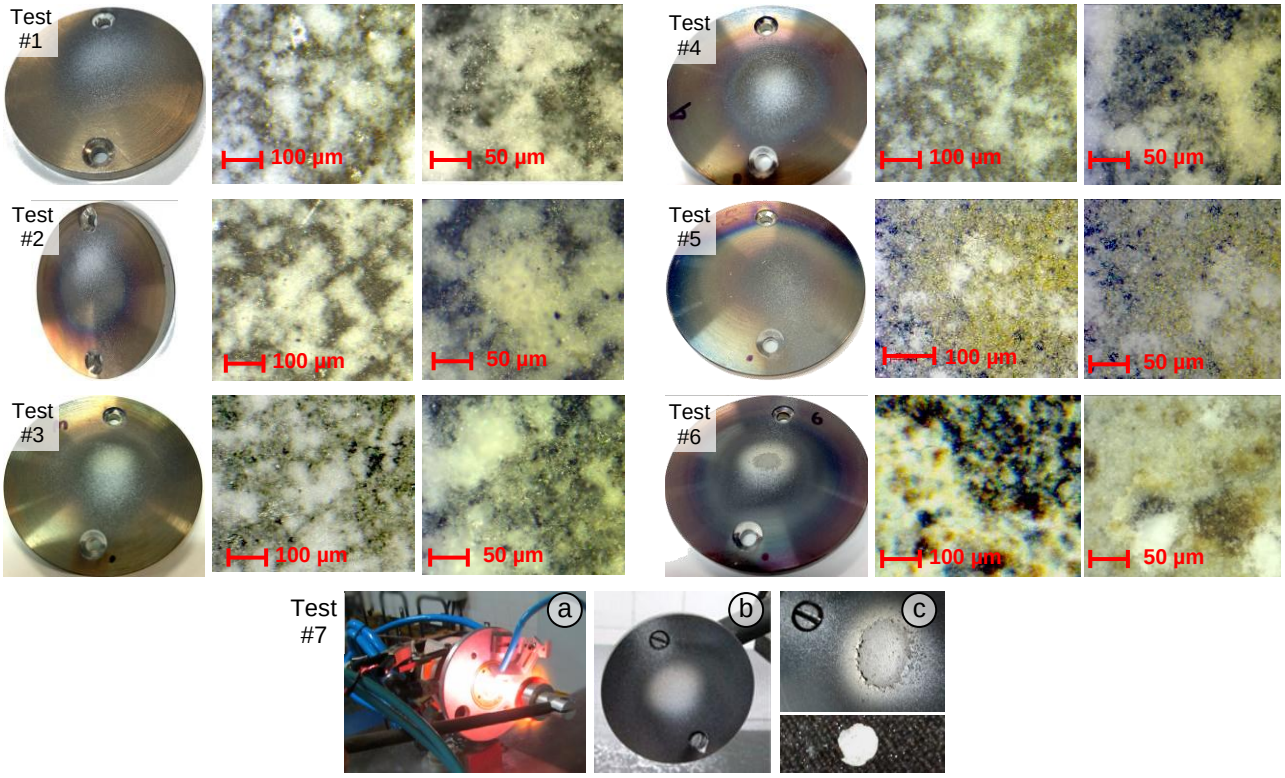


Figure 14. Coatings obtained by varying the spray parameters

| Test | Samples | d (cm) | $t_d$ (s) | Nº layers |
|---|---|---|---|---|
| #08 | A09 | 7.0 | 15 | 6 |
| #09 | A10 | 7.0 | 15 | 6 |
| #10 | A11 | 7.0 | 10 | 8 |
| #11 | A12 | 6.5 | 10 | 7 |
| #12 | A13 | 6.5 | 9 | 7 |
| #13 | A14 | 6.5 | 8 | 7 |
| #14 | A15 | 6.5 | 4 | 8 |
| #15 | A16 | 6.5 | 5 | 8 |
| #16 | A17 | 6.5 | 6 | 8 |
| #17 | A18 | 6.5 | 7 | 8 |

Note: The gray font refers to values that remained the same as in the previous test.

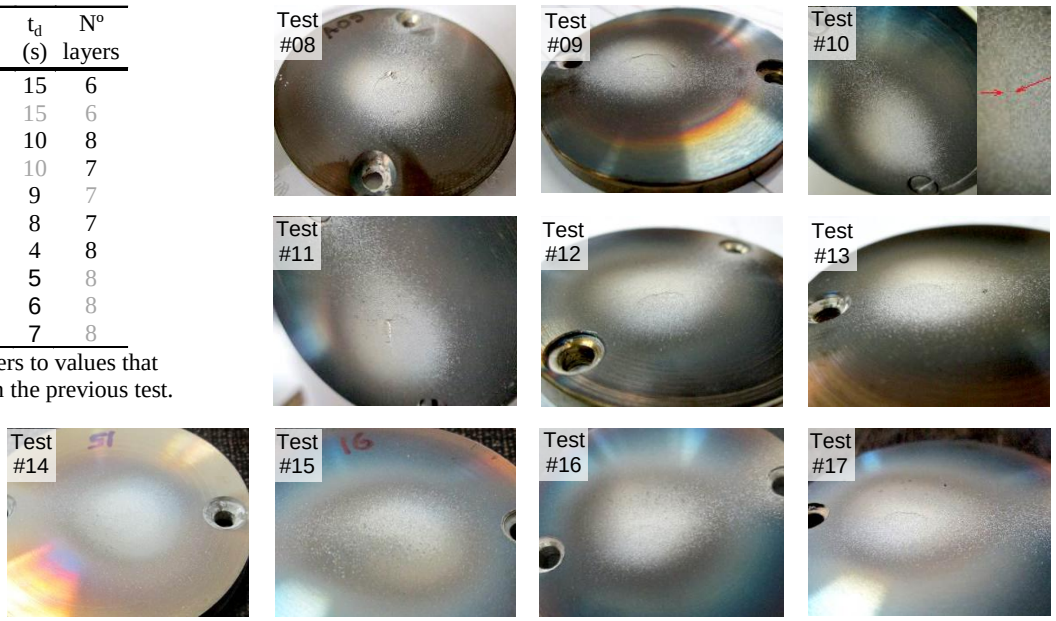


Figure 15. Results of multilayer coatings

### 3.4 Velocity and temperature of the powder particles

The DPV analysis was performed to same setup used on Test #7 in the table 1. The mean temperature of the particles was $2.49 \pm 0.19 \times 10^3$ °C ($\pm 1\sigma$). Thus, for $2\sigma$, 95% of the particles would be in the range of $2.11\text{-}2.87 \times 10^3$ °C, above of the alumina melting point (2,072 °C) (Patnaik, 2003). The mean velocity of the particles was $527 \pm 66$ m/s ($\pm 1\sigma$) showing that even with the powder flow being directed against the plasma jet, due the reduction of diameter in torch anode, the flow of the plasma jet was able to change the direction of the axial velocity of the powder at supersonic velocity toward the substrate. The speed which the molten particles reach the substrate contributes to splat conformation and fixation to the substrate and also between the coating layers.

## 4. CONCLUSIONS

This work showed that plasma jet temperature and powder flow rate control are initial points that have be mastered in the implementation of a powder thermal spray system. There is a diversity of parameters that involve the obtaining of a thick and free defects coating like delamination and cracks. The difference between the thermal expansion coefficients of the coating materials and the substrate is relevant, and deserves initial attention in the process. This will limit the exposure of the substrate to the plasma jet. On the other hand, longer residence times of the ceramic particles in the plasma jet and a higher gas temperature result a thicker coating with less accumulation of non-molten particles. The coatings deposited in this work consisted of a spot spraying that was performed to determine the essential parameters that are required for the development of thermal spray system. In order to obtain a coating of constant thickness, it would be necessary to further include an area sweep feature for the spray, either by moving the plasma torch into two (most common) coordinate axes or the substrate.

## 5. ACKNOWLEDGEMENTS

The authors would like to thank the AEB and CNPq for funding the research.

## 6. REFERENCES

Fauchais P., 2004. "Understanding plasma spraying". *J Phys D Appl Phys*, Vol. 37, pp. R86–R108

Fauchais P.L., Heberlein J.V.R., Boulos M., 2014. Thermal Spray Fundamentals: From Powder to Part. Springer, New York

Li H.Q., Wang Q.M., Jiang S.M., Ma J., Gong J., Sun C., 2011. "Oxidation and interfacial fracture behaviour of NiCrAlY/Al2O3 coatings on an orthorhombic-Ti2AlNb alloy". *Corros Sci*, Vol. 53, pp. 1097–1106

Mauer G., Vaßen R., Zimmermann S., Biermordt T., Heinrich M., Marques J.-L., Landes K., Schein J., 2013. "Investigation and Comparison of In-Flight Particle Velocity During the Plasma-Spray Process as Measured by Laser Doppler Anemometry and DPV-2000". *J Therm Spray Technol*, Vol. 22, pp. 892–900

Miranda F., Caliari F., Essiptchouk A., Pertraconi G., 2018. "Atmospheric Plasma Spray Processes: From Micro to Nanostructures". In: Atmospheric Pressure Plasma [Working Title]. IntechOpen

P. Fauchais; M. I. Boulos and E. Pfender, 1994. Thermal Plasmas - Fundamentals and Applications. New York

Patnaik P., 2003. Handbook of Inorganic Chemicals

Pawlowski L., 2008. The science and engineering of thermal spray coatings. John Wiley & Sons Ltd, Chichester, UK

Silva R.J., 2011. "Plasma térmico para ablação de materiais utilizados como escudo de proteção térmica em sistemas aeroespaciais". Instituto Tecnológico de Aeronáutica

Solonenko O., 2003. Thermal Plasma Torches and Technologies: Plasma Torches, Basic Studies and Design. Cambridge International Science Publishing, Cambridge - UK

Tucker Jr. R.C., 2013. ASM Handbook, Volume 05A - Thermal Spray Technology

Xie L., Ma X., Ozturk A., Jordan E.H., Padture N.P., Cetegen B.M., Xiao D.T., Gell M., 2004. "Processing parameter effects on solution precursor plasma spray process spray patterns". *Surf Coatings Technol*, Vol. 183, pp. 51–61

## 7. RESPONSIBILITY NOTICE

The authors are the only responsible for the printed material included in this paper.